

# $Z'$ -portal right-handed neutrino dark matter in the minimal $U(1)_X$ extended Standard Model

Nobuchika Okada <sup>a</sup> and Satomi Okada <sup>b</sup>

<sup>a</sup>*Department of Physics and Astronomy, University of Alabama, Tuscaloosa, AL35487, USA*

<sup>b</sup>*Graduate School of Science and Engineering, Yamagata University,  
Yamagata 990-8560, Japan*

## Abstract

We consider a concise dark matter (DM) scenario in the context of a non-exotic  $U(1)$  extension of the Standard Model (SM), where a new  $U(1)_X$  gauge symmetry is introduced along with three generation of right-handed neutrinos (RHNs) and an SM gauge singlet Higgs field. The model is a generalization of the minimal gauged  $U(1)_{B-L}$  (baryon number minus lepton number) extension of the SM, in which the extra  $U(1)_X$  gauge symmetry is expressed as a linear combination of the SM  $U(1)_Y$  and  $U(1)_{B-L}$  gauge symmetries. We introduce a  $Z_2$ -parity and assign an odd-parity only for one RHN among all particles, so that this  $Z_2$ -odd RHN plays a role of DM. The so-called minimal seesaw mechanism is implemented in this model with only two  $Z_2$ -even RHNs. In this context, we investigate physics of the RHN DM, focusing on the case that this DM particle communicates with the SM particles through the  $U(1)_X$  gauge boson ( $Z'$  boson). This “ $Z'$ -portal RHN DM” scenario is controlled by only three free parameters: the  $U(1)_X$  gauge coupling ( $\alpha_X$ ), the  $Z'$  boson mass ( $m_{Z'}$ ), and the  $U(1)_X$  charge of the SM Higgs doublet ( $x_H$ ). We consider various phenomenological constraints to identify a phenomenologically viable parameter space. The most important constraints are the observed DM relic abundance and the latest LHC Run-2 results on the search for a narrow resonance with the di-lepton final state. We find that these are complementary with each other and narrow the allowed parameter region, leading to the lower mass bound of  $m_{Z'} \gtrsim 2.7$  TeV.

## I. INTRODUCTION

Neutrino masses and a suitable candidate for the dark matter are the major missing pieces in the Standard Model (SM), which require us to extend the SM. The minimal  $B - L$  model [1–6] is a simple, well-motivated extension of the SM to incorporate the neutrino masses, where the global  $U(1)_{B-L}$  (baryon number minus lepton number) symmetry in the SM is gauged. In the presence of the three right-handed neutrinos (RHNs) the model is free from all the gauge and gravitational anomalies. Associated with the spontaneous  $B - L$  gauge symmetry breaking by a vacuum expectation value (VEV) of the  $B - L$  Higgs field, the RHNs and the  $B - L$  gauge boson ( $Z'$  boson) acquire their masses. With the generated Majorana masses for the RHNs, the seesaw mechanism [7–11] is implemented, and the light SM neutrino mass is generated after the electroweak symmetry breaking. The mass spectrum of the new particles introduced in the minimal  $B - L$  model (the  $Z'$  boson, the Majorana RHNs and the  $B - L$  Higgs boson) is controlled by the  $B - L$  gauge symmetry breaking scale. If the breaking scale lies around the TeV scale, the  $B - L$  model can be tested at the Large Hadron Collider (LHC).

Among various possibilities, a concise way of introducing a dark matter (DM) candidate in the minimal  $B - L$  model has been proposed in Ref. [12]. Instead of extending the minimal particle content, a  $Z_2$ -parity is introduced and an odd-parity is assigned to only one RHN while even-parities are assigned to all the other fields.<sup>1</sup> Hence, the parity-odd RHN serves as the DM. On the other hand, two parity-even RHNs account for the neutrino mass generation via the seesaw mechanism. This system is nothing but the so-called minimal seesaw [14, 15], which is the minimal setup to reproduce the observed neutrino oscillation data with a prediction of one massless neutrino as well as the observed baryon asymmetry in the universe through leptogenesis [16].

There are two ways for the RHN DM to communicate with the SM particles. One is through two Higgs bosons, which are expressed as linear combinations of the SM Higgs and the  $B - L$  Higgs bosons after the breaking of the  $U(1)_{B-L}$  and the electroweak gauge symmetries. The DM phenomenology for this case has been analyzed in [12, 17, 18]. The other way is that the interactions between the DM and the SM particles are mediated by the  $Z'$  boson. This class of DM scenario is called “ $Z'$ -portal DM” and has been attracting a lot of attention recently. In the scenario, a DM particle is introduced along with an electric-charge neutral vector field ( $Z'$  boson) in an extension of the SM with the so-called Dark Sector [19–22] or new gauge interactions [23–49]. The mediator  $Z'$  boson allows us to investigate a variety of DM physics, such as the DM relic abundance and the direct/indirect DM search. A remarkable feature of the

---

<sup>1</sup> We can consider the  $Z_2$ -parity as an emergent global symmetry in the limit of vanishing Dirac Yukawa couplings [13].

scenario is that the  $Z'$  boson resonance search at the LHC is complementary to the cosmological observations of the  $Z'$ -portal DM in identifying a phenomenologically viable parameter region.

Recently, the minimal  $B - L$  model with the RHN DM has been investigated in the light of the LHC Run-2 results [40]. Here, the RHN DM communicates with the SM particles mainly through the  $Z'$  gauge boson, and hence it is the  $Z'$ -portal DM scenario. In the model, the DM physics is controlled by only two free parameters, the  $B - L$  gauge coupling and the  $Z'$  boson mass. It has been found that the constraint from the observed DM relic abundance leads to a lower bound on the gauge coupling as a function of the  $Z'$  boson mass. On the other hand, the cross section of  $Z'$  boson production at the LHC is also determined by the same two free parameters. The LHC Run-2 results on search for a narrow resonance with the di-lepton final states have been interpreted to obtain the upper bound on the gauge coupling as a function of the  $Z'$  boson mass. Combining the two results, an allowed parameter region has been identified to obtain the lower bound of  $m_{Z'} \gtrsim 2.5$  TeV. In deriving the allowed parameter region, a complementarity between the cosmological and the collider constraints was essential.

In this paper, we generalize the minimal  $B - L$  model to the so-called non-exotic  $U(1)_X$  extension of the SM [50]. The non-exotic  $U(1)_X$  model is the most general extension of the SM with an extra anomaly-free  $U(1)$  gauge symmetry, which is described as a linear combination of the SM  $U(1)_Y$  and the  $U(1)_{B-L}$  gauge groups. The particle content of the model is the same as the one in the minimal  $B - L$  model except for the generalization of the  $U(1)_X$  charge assignment for particles. Hence we can easily extend the minimal  $B - L$  model with the RHN DM to the non-exotic  $U(1)_X$  case. In this context, we perform detailed analysis to identify a phenomenologically viable parameter region through the complementarity between the DM physics and the LHC Run-2 results. Because of the  $U(1)_X$  generalization, the  $Z'$  boson couplings with the SM particles are modified and the resultant parameter region is found to be quite different from the one obtained in Ref. [40]. For the LHC Run-2 results, we employ the most recent results reported by the ATLAS and the CMS collaborations in 2016 [51, 52].

This paper is organized as follows. In the next section, we define the minimal non-exotic  $U(1)_X$  extension of the SM with the  $Z'$ -portal RHN DM. In Sec. III, we analyze the DM relic abundance and identify a model parameter region to satisfy the observed DM relic abundance. In Sec. IV, we consider the results by the ATLAS and the CMS collaborations at the LHC Run-2 on the search for a narrow resonance with the di-lepton final states. We interpret the results into the constraints on the  $Z'$  boson production in the minimal non-exotic  $U(1)_X$  model. Combining all the constraints, we identify the allowed parameter regions in Sec. V. The last section is devoted to conclusions.

	SU(3) <sub>c</sub>	SU(2) <sub>L</sub>	U(1) <sub>Y</sub>	U(1) <sub>X</sub>	Z <sub>2</sub>
$q_L^i$	<b>3</b>	<b>2</b>	1/6	$(1/6)x_H + (1/3)x_\Phi$	+
$u_R^i$	<b>3</b>	<b>1</b>	2/3	$(2/3)x_H + (1/3)x_\Phi$	+
$d_R^i$	<b>3</b>	<b>1</b>	-1/3	$-(1/3)x_H + (1/3)x_\Phi$	+
$\ell_L^i$	<b>1</b>	<b>2</b>	-1/2	$(-1/2)x_H - x_\Phi$	+
$e_R^i$	<b>1</b>	<b>1</b>	-1	$-x_H - x_\Phi$	+
$H$	<b>1</b>	<b>2</b>	-1/2	$(-1/2)x_H$	+
$N_R^j$	<b>1</b>	<b>1</b>	0	$-x_\Phi$	+
$N_R$	<b>1</b>	<b>1</b>	0	$-x_\Phi$	-
$\Phi$	<b>1</b>	<b>1</b>	0	$+2x_\Phi$	+

TABLE I. The particle content of the minimal U(1)<sub>X</sub> extended SM with Z<sub>2</sub> parity. In addition to the SM particle content ( $i = 1, 2, 3$ ), the three RHNs ( $N_R^j$  ( $j = 1, 2$ ) and  $N_R$ ) and the U(1)<sub>X</sub> Higgs field ( $\Phi$ ) are introduced. Because of the Z<sub>2</sub> parity assignment shown here, the  $N_R$  is a unique (cold) DM candidate. The extra U(1)<sub>X</sub> gauge group is defined with a linear combination of the SM U(1)<sub>Y</sub> and the U(1)<sub>B-L</sub> gauge groups, and the U(1)<sub>X</sub> charges of fields are determined by two real parameters,  $x_H$  and  $x_\Phi$ . Without loss of generality, we fix  $x_\Phi = 1$  throughout this paper.

## II. THE MINIMAL NON-EXOTIC U(1)<sub>X</sub> MODEL WITH RHN DM

We first define our model by the particle content listed on Table I. The U(1)<sub>X</sub> gauge group is identified with a linear combination of the SM U(1)<sub>Y</sub> and the U(1)<sub>B-L</sub> gauge groups, and hence the U(1)<sub>X</sub> charges of fields are determined by two real parameters,  $x_H$  and  $x_\Phi$ . Note that in the model the charge  $x_\Phi$  always appears as a product with the U(1)<sub>X</sub> gauge coupling and it is not an independent free parameter. Hence, we fix  $x_\Phi = 1$  throughout this paper. In this way, we reproduce the minimal  $B - L$  model with the conventional charge assignment as the limit of  $x_H \rightarrow 0$ . The limit of  $x_H \rightarrow +\infty$  ( $-\infty$ ) indicates that the U(1)<sub>X</sub> is (anti-)aligned to the U(1)<sub>Y</sub> direction. The anomaly structure of the model is the same as the minimal  $B - L$  model and the model is free from all the gauge and the gravitational anomalies in the presence of the three RHNs. The introduction of the Z<sub>2</sub>-parity is crucial to incorporate a DM candidate in the model while keeping the minimality of the particle content. The conservation of the Z<sub>2</sub>-parity ensures the stability of the Z<sub>2</sub>-odd RHN, and therefore it is a unique DM candidate in the model.

The Yukawa sector of the SM is extended to have

$$\mathcal{L}_{Yukawa} \supset - \sum_{i=1}^3 \sum_{j=1}^2 Y_D^{ij} \overline{\ell}_L^i H N_R^j - \frac{1}{2} \sum_{k=1}^2 Y_N^k \Phi \overline{N_R^k} N_R^k - \frac{1}{2} Y_N \Phi \overline{N_R} N_R + \text{h.c.}, \quad (1)$$

where the first term is the neutrino Dirac Yukawa coupling, and the second and third terms are the Majorana Yukawa couplings. Without loss of generality, the Majorana Yukawa couplings are

already diagonalized in our basis. Note that because of the  $Z_2$ -parity, only the two generation RHNs are involved in the neutrino Dirac Yukawa coupling. Once the  $U(1)_X$  Higgs field  $\Phi$  develops a nonzero VEV, the  $U(1)_X$  gauge symmetry is broken and the Majorana mass terms for the RHNs are generated. Then, the seesaw mechanism is automatically implemented in the model after the electroweak symmetry breaking. Because of the  $Z_2$ -parity, only two generation RHNs are relevant to the seesaw mechanism. Even with two RHNs, the Yukawa coupling constants  $Y_D^{ij}$  and  $Y_N^k$  possess the degrees of freedom large enough to reproduce the neutrino oscillation data with a prediction of one massless eigenstate. The baryon asymmetry in the universe can also be reproduced with the two RHNs [15] (see, for example, Ref. [53] for detailed analysis of leptogenesis at the TeV scale with two RHNs).

The renormalizable scalar potential for the SM Higgs doublet ( $H$ ) and the  $U(1)_X$  Higgs fields is given by

$$V = \lambda_H \left( H^\dagger H - \frac{v^2}{2} \right)^2 + \lambda_\Phi \left( \Phi^\dagger \Phi - \frac{v_X^2}{2} \right)^2 + \lambda_{\text{mix}} \left( H^\dagger H - \frac{v^2}{2} \right) \left( \Phi^\dagger \Phi - \frac{v_X^2}{2} \right), \quad (2)$$

where all quartic couplings are chosen to be positive. At the potential minimum, the Higgs fields develop their VEVs as

$$\langle H \rangle = \begin{pmatrix} \frac{v}{\sqrt{2}} \\ 0 \end{pmatrix}, \quad \langle \Phi \rangle = \frac{v_X}{\sqrt{2}}. \quad (3)$$

In this paper, we assume  $\lambda_{\text{mix}} \ll 1$ , so that the mixing between the SM Higgs boson and the  $U(1)_X$  Higgs boson are negligibly small.<sup>2</sup> Hence, the RHN DM communicates with the SM particles only through the  $Z'$  boson. Associated with the  $U(1)_X$  symmetry breaking, the Majorana neutrinos  $N_R^j$  ( $j = 1, 2$ ), the DM particle  $N_R$  and the  $Z'$  gauge boson acquire their masses as

$$m_N^j = \frac{Y_N^j}{\sqrt{2}} v_X, \quad m_{DM} = \frac{Y_N}{\sqrt{2}} v_X, \quad m_{Z'} = g_X \sqrt{4v_X^2 + \frac{v^2}{4}} \simeq 2g_X v_X, \quad (4)$$

where  $g_X$  is the  $U(1)_X$  gauge coupling, and we have used the LEP constraint [54, 55]  $v_X^2 \gg v^2$ . Because of the LEP constraint, the mass mixing of the  $Z'$  boson with the SM  $Z$  boson is very small, and we neglect it in our analysis in this paper.

Assuming  $\lambda_{\text{mix}} \ll 1$ , we focus on the  $Z'$ -portal nature of the RHN DM. In this case, only four free parameters ( $g_X$ ,  $m_{Z'}$ ,  $m_{DM}$ , and  $x_H$ ) are involved in our analysis. As we will discuss in the next section, it turns out that the condition of  $m_{DM} \simeq m_{Z'}/2$  must be satisfied to reproduce the observed DM relic abundance. Thus,  $m_{DM}$  does not work as an independent parameter, so that our results are described by only three free parameters.

<sup>2</sup> This assumption is, in fact, not essential. When  $\lambda_{\text{mix}}$  is sizable, the RHN DM can communicate with the SM particles also through the Higgs bosons. This so-called Higgs portal RHN DM case has been analyzed in [12, 17, 18] and it has been shown that the RHN DM mass is required to be close to a half of either one of the Higgs boson masses in order to reproduce the observed relic abundance. Such a parameter region is distinguishable from that in our  $Z'$ -portal RHN DM<sub>4</sub> case, and we can investigate the two cases separately.

### III. COSMOLOGICAL CONSTRAINTS ON $Z'$ -PORTAL RHN DM.

In the Planck satellite experiments, the DM relic abundance is measured at the 68% limit as [56]

$$\Omega_{DM}h^2 = 0.1198 \pm 0.0015. \quad (5)$$

In this section, we evaluate the DM relic abundance and identify an allowed parameter region to satisfy the upper bound of  $\Omega_{DM}h^2 \leq 0.1213$ . The DM relic abundance is evaluated by integrating the Boltzmann equation given by

$$\frac{dY}{dx} = -\frac{xs\langle\sigma v\rangle}{H(m_{DM})}(Y^2 - Y_{EQ}^2), \quad (6)$$

where the temperature of the universe is normalized by the mass of the RHN DM as  $x = m_{DM}/T$ ,  $H(m_{DM})$  is the Hubble parameter at  $T = m_{DM}$ ,  $Y$  is the yield (the ratio of the DM number density to the entropy density  $s$ ) of the RHN DM,  $Y_{EQ}$  is the yield of the DM particle in thermal equilibrium, and  $\langle\sigma v\rangle$  is the thermal average of the DM annihilation cross section times relative velocity ( $v$ ). Explicit formulas of the quantities involved in the Boltzmann equation are as follows:

$$s = \frac{2\pi^2}{45}g_\star\frac{m_{DM}^3}{x^3}, \quad H(m_{DM}) = \sqrt{\frac{\pi^2}{90}g_\star}\frac{m_{DM}^2}{M_P}, \quad sY_{EQ} = \frac{g_{DM}}{2\pi^2}\frac{m_{DM}^3}{x}K_2(x), \quad (7)$$

where  $M_P = 2.44 \times 10^{18}$  GeV is the reduced Planck mass,  $g_{DM} = 2$  is the number of degrees of freedom for the DM particle,  $g_\star$  is the effective total number of degrees of freedom for the particles in thermal equilibrium (in the following analysis, we use  $g_\star = 106.75$  for the SM particles), and  $K_2$  is the modified Bessel function of the second kind. In our  $Z'$ -portal DM scenario, a DM pair annihilates into the SM particles through the  $Z'$  boson exchange in the  $s$ -channel. The thermal average of the annihilation cross section is given by

$$\langle\sigma v\rangle = (sY_{EQ})^{-2}g_{DM}^2\frac{m_{DM}}{64\pi^4x}\int_{4m_{DM}^2}^{\infty}ds\hat{\sigma}(s)\sqrt{s}K_1\left(\frac{x\sqrt{s}}{m_{DM}}\right), \quad (8)$$

where  $\hat{\sigma}(s) = 2(s - 4m_{DM}^2)\sigma(s)$  is the reduced cross section with the total annihilation cross section  $\sigma(s)$ , and  $K_1$  is the modified Bessel function of the first kind. The total cross section of the DM pair annihilation process  $NN \rightarrow Z' \rightarrow f\bar{f}$  ( $f$  denotes the SM fermions) is calculated as

$$\sigma(s) = \frac{\pi}{3}\alpha_X^2\frac{\sqrt{s(s - 4m_{DM}^2)}}{(s - m_{Z'}^2)^2 + m_{Z'}^2\Gamma_{Z'}^2}F(x_H), \quad (9)$$

where

$$F(x_H) = 13 + 16x_H + 10x_H^2 = 10(x_H + 0.8)^2 + 6.6, \quad (10)$$

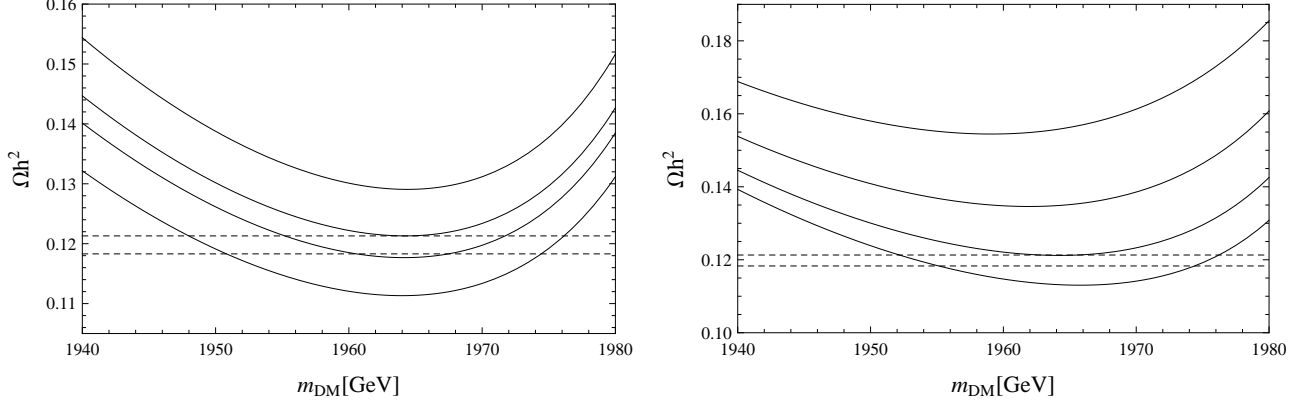


FIG. 1. The relic abundance of the  $Z'$ -portal RHN DM as a function of its mass ( $m_{DM}$ ) for  $m_{Z'} = 4$  TeV. In the left panel, we have fixed  $x_H = 0$  (the minimal  $B - L$  model limit) and shown the relic abundance for various values of the gauge coupling,  $\alpha_X = 0.025, 0.027, 0.028$  and  $0.030$  (solid lines from top to bottom). In the right panel, we have fixed  $\alpha_X = 0.027$  and shown the relic abundance for various values of  $x_H = -0.8, 0, 0.5$  and  $1.0$  (solid lines from bottom to top). The two horizontal lines denote the range of the observed DM relic density,  $0.1183 \leq \Omega_{DM} h^2 \leq 0.1213$  in Eq. (5).

and the total decay width of  $Z'$  boson is given by

$$\Gamma_{Z'} = \frac{\alpha_X}{6} m_{Z'} \left[ F(x_H) + \left( 1 - \frac{4m_{DM}^2}{m_{Z'}^2} \right)^{\frac{3}{2}} \theta \left( \frac{m_{Z'}^2}{m_{DM}^2} - 4 \right) \right]. \quad (11)$$

Here, we have neglected all SM fermion masses and assumed  $m_N^j > m_{Z'}/2$ , for simplicity.

Now we solve the Boltzmann equation numerically, and find the asymptotic value of the yield  $Y(\infty)$  to evaluate the present DM relic density as

$$\Omega_{DM} h^2 = \frac{m_{DM} s_0 Y(\infty)}{\rho_c / h^2}, \quad (12)$$

where  $s_0 = 2890 \text{ cm}^{-3}$  is the entropy density of the present universe, and  $\rho_c / h^2 = 1.05 \times 10^{-5} \text{ GeV/cm}^3$  is the critical density. Our analysis involves four parameters, namely  $\alpha_X = g_X^2 / (4\pi)$ ,  $m_{Z'}$ ,  $m_{DM}$  and  $x_H$ . For  $m_{Z'} = 4 \text{ TeV}$ , we show in Fig. 1 the resultant DM relic abundance as a function of the DM mass, along with the range of the observed DM relic abundance,  $0.1183 \leq \Omega_{DM} h^2 \leq 0.1213$  [56] (two horizontal dashed lines). In the left panel, we have fixed  $x_H = 0$ , which is the minimal  $B - L$  model limit. The solid lines from top to bottom show the resultant DM relic abundances for various values of the gauge coupling,  $\alpha_X = 0.025, 0.027, 0.028$  and  $0.030$ . The plots indicate the lower bound on  $\alpha_X \geq 0.027$  for  $m_{Z'} = 4 \text{ TeV}$  and  $x_H = 0$  in order to be able to reproduce the observed relic abundance. In addition, we can see that the enhancement of the DM annihilation cross section via the  $Z'$  boson resonance is necessary to satisfy the cosmological constraint and hence,  $m_{DM} \simeq m_{Z'}/2$ . The right panel shows our

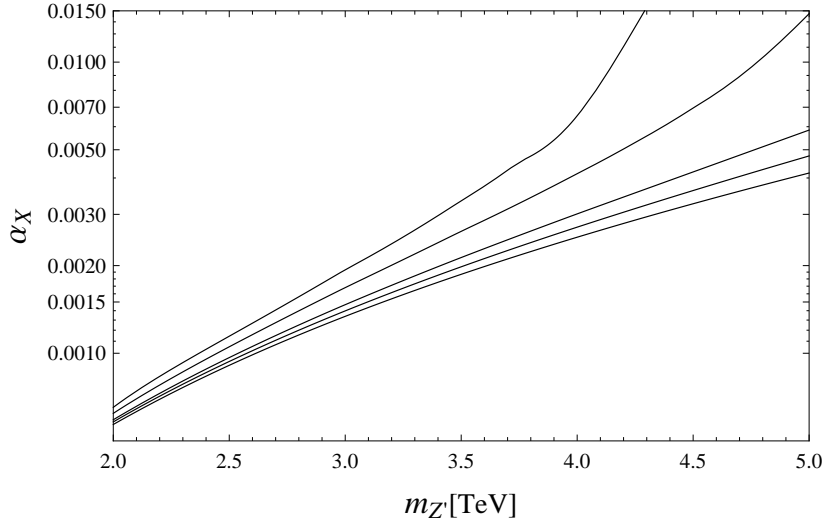


FIG. 2. The lower bounds on  $\alpha_X$  as a function of  $m_{Z'}$  for various values of  $x_H$ , to satisfy the cosmological constraint of  $0.1183 \leq \Omega_{DM} h^2 \leq 0.1213$ . The solid lines from top to bottom corresponds to  $x_H = -3, +1, -2, 0$  and  $-1$ , respectively. As the input  $x_H$  value is going away from the point of  $x_H = -0.8$ , the lower bound on  $\alpha_X$  is increasing.

results for various values of  $x_H$  with the fixed  $\alpha_X = 0.027$ . The solid lines from bottom to top correspond to the results for  $x_H = -0.8, 0, 0.5$  and  $1.0$ , respectively. From Eqs. (8)-(11), we can see that the DM annihilation cross section for  $m_{DM} \simeq m_{Z'}/2$  is proportional to  $1/F(x_H)$ . Therefore, the maximum annihilation cross section for the fixed values of  $\alpha_X$ ,  $m_{Z'}$  and  $m_{DM} \simeq m_{Z'}/2$  is achieved for  $x_H = -0.8$ . Since the function  $F(x_H)$  is symmetric about the point of  $x_H = -0.8$ , the results shown in the left panel indicate the constraint  $-1.6 \leq x_H \leq 0$  to satisfy the cosmological bound for the fixed values of  $m_{Z'} = 4$  TeV and  $\alpha_X = 0.027$ .

In Fig. 2 we show the lower bounds on  $\alpha_X$  as a function of  $m_{Z'}$  for various values of  $x_H$ , to reproduce the observed DM relic abundance in the range of  $0.1183 \leq \Omega_{DM} h^2 \leq 0.1213$ . The solid lines from top to bottom corresponds to  $x_H = -3, +1, -2, 0$  and  $-1$ , respectively. For fixed  $\alpha_X$  and  $m_{Z'}$ , the DM annihilation cross section becomes maximum for  $x_H \simeq -0.8$  with the minimum  $Z'$  boson decay width. As an input  $x_H$  value is going away from the point of  $x_H = -0.8$ , the decay width becomes larger and the DM annihilation cross section is reducing. As a result, the lower bound on the gauge coupling is increasing.

#### IV. LHC RUN-2 CONSTRAINTS

In 2015, the LHC Run-2 started its operation with a 13 TeV collider energy. The most recent results by the ATLAS and the CMS collaborations with the combined 2015 and 2016 data were

reported at the ICHEP 2016 conference. The ATLAS and the CMS collaborations continue their search for  $Z'$  boson resonance with di-lepton final states at the LHC Run-2. Their results have shown significant improvements for the upper limits of the  $Z'$  boson production cross section [51, 52] from those obtained by the LHC Run-1 [57, 58]. In this section, we will employ the most recent LHC Run-2 results to derive LHC constraints on the model parameters,  $\alpha_X$ ,  $m_{Z'}$  and  $x_H$ .

Let us calculate the cross section for the process  $pp \rightarrow Z' + X \rightarrow \ell^+ \ell^- + X$ . The differential cross section with respect to the invariant mass  $M_{\ell\ell}$  of the final state di-lepton is given by

$$\frac{d\sigma}{dM_{\ell\ell}} = \sum_{q,\bar{q}} \int_{\frac{M_{\ell\ell}^2}{E_{\text{CM}}^2}}^1 dx \frac{2M_{\ell\ell}}{xE_{\text{CM}}^2} f_q(x, Q^2) f_{\bar{q}}\left(\frac{M_{\ell\ell}^2}{xE_{\text{CM}}^2}, Q^2\right) \hat{\sigma}(q\bar{q} \rightarrow Z' \rightarrow \ell^+ \ell^-), \quad (13)$$

where  $f_q$  is the parton distribution function for a parton (quark) “ $q$ ”, and  $E_{\text{CM}} = 13$  TeV is the center-of-mass energy of the LHC Run-2. In our numerical analysis, we employ CTEQ6L [59] for the parton distribution functions with the factorization scale  $Q = m_{Z'}$ . Here, the cross section for the colliding partons is given by

$$\hat{\sigma}(q\bar{q} \rightarrow Z' \rightarrow \ell^+ \ell^-) = \frac{\pi}{1296} \alpha_X^2 \frac{M_{\ell\ell}^2}{(M_{\ell\ell}^2 - m_{Z'}^2)^2 + m_{Z'}^2 \Gamma_{Z'}^2} F_{q\ell}(x_H), \quad (14)$$

where the function  $F_{q\ell}(x_H)$  is given by

$$\begin{aligned} F_{u\ell}(x_H) &= (8 + 20x_H + 17x_H^2)(8 + 12x_H + 5x_H^2), \\ F_{d\ell}(x_H) &= (8 - 4x_H + 5x_H^2)(8 + 12x_H + 5x_H^2) \end{aligned} \quad (15)$$

for  $q$  being the up-type ( $u$ ) and down-type ( $d$ ) quarks, respectively. By integrating the differential cross section over a range of  $M_{\ell\ell}$  set by the ATLAS and the CMS analysis, respectively, we obtain the cross section to be compared with the upper bounds obtained by the ATLAS and the CMS collaborations.

In the analysis by the ATLAS and the CMS collaborations, the so-called sequential SM  $Z'$  ( $Z'_{SSM}$ ) model [61] has been considered as a reference model. We first analyze the sequential  $Z'$  model to check a consistency of our analysis with the one by the ATLAS collaboration. In the sequential  $Z'$  model, the  $Z'_{SSM}$  boson has exactly the same couplings with quarks and leptons as the SM  $Z$  boson. With the couplings, we calculate the cross section of the process  $pp \rightarrow Z'_{SSM} + X \rightarrow \ell^+ \ell^- + X$  like Eq. (13). By integrating the differential cross section in the region of  $128 \text{ GeV} \leq M_{\ell\ell} \leq 6000 \text{ GeV}$  [57], we obtain the cross section of the di-lepton production process as a function of  $Z'_{SSM}$  boson mass. Our result is shown as a solid line in the left panel on Fig. 3, along with the plot presented by the ATLAS collaboration [51, 60]. In the ATLAS paper [51], the lower limit of the  $Z'_{SSM}$  boson mass is found to be 4.05 TeV, which

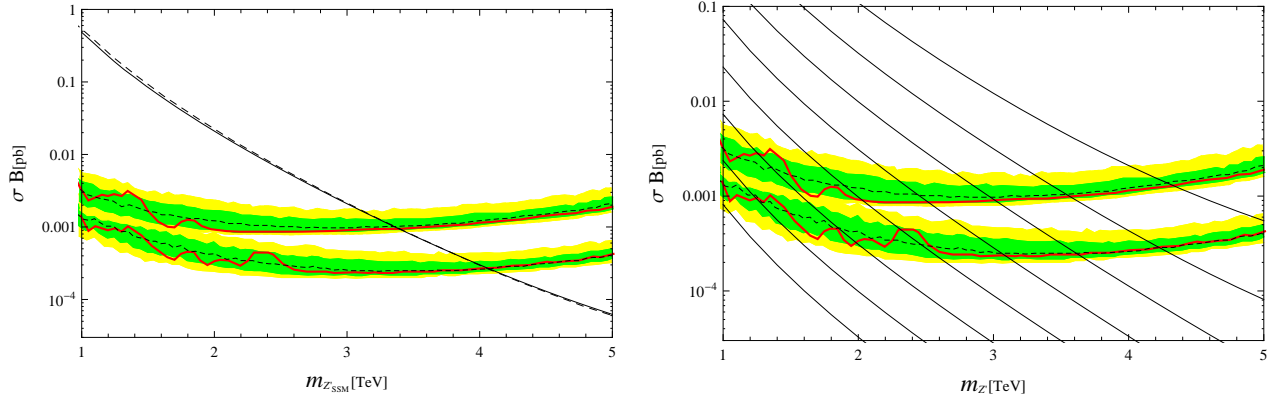


FIG. 3. Left panel: the cross section as a function of the  $Z'_{SSM}$  mass (solid line) with  $k = 1.28$ , along with the ATLAS results in 2016 [51] and 2015 [60] from the combined di-electron and di-muon channels. Right panel: the cross sections calculated for various values of  $\alpha_X$  with  $k = 1.28$ , for the minimal  $B - L$  model limit ( $x_H = 0$ ). The solid lines from left to right correspond to  $\alpha_X = 10^{-5}$ ,  $10^{-4.5}$ ,  $10^{-4}$ ,  $10^{-3.5}$ ,  $10^{-3}$ ,  $10^{-2.5}$ ,  $10^{-2}$ , and  $10^{-1.5}$ , respectively.

is read off from the intersection point of the theoretical prediction (diagonal dashed line) and the experimental cross section bound (lower horizontal solid curve (in red)). Here, we have also shown the plot presented in Ref. [60] (upper horizontal solid curve (in red)). We can see the dramatic improvement from the 2015 results [60] to the 2016 results [51]. In order to take into account the difference of the parton distribution functions used in the ATLAS and our analysis and QCD corrections of the process, we have scaled our resultant cross section by a factor  $k = 1.28$ , with which we can obtain the same lower limit of the  $Z'_{SSM}$  boson mass as 4.05 TeV. We can see that our result with the factor of  $k = 1.28$  (solid line) is very consistent with the theoretical prediction (diagonal dashed line) presented in Ref. [51]. This factor is used in our analysis of the  $Z'$  boson production process in the following.

Now we calculate the cross section of the process  $pp \rightarrow Z' + X \rightarrow \ell^+\ell^- + X$  for various values of  $\alpha_X$ ,  $m_{Z'}$  and  $x_H$ . For  $x_H = 0$  (the minimal  $B - L$  model limit), we show our results in the right panel of Fig. 3, along with the plots in the ATLAS papers [51, 60]. The diagonal solid lines from left to right correspond to  $\alpha_X = 10^{-5}$ ,  $10^{-4.5}$ ,  $10^{-4}$ ,  $10^{-3.5}$ ,  $10^{-3}$ ,  $10^{-2.5}$ ,  $10^{-2}$ , and  $10^{-1.5}$ . From the intersections of the lower horizontal curve (in red) and diagonal solid lines, we can read off the lower bounds on the  $Z'$  boson mass for the corresponding  $\alpha_X$  values. For example,  $m_{Z'} > 3.1$  TeV for  $\alpha_X = 0.001$ . In this way, we have obtained the upper bound on  $\alpha_X$  as a function of the  $Z'$  boson mass. For various values of  $x_H$  we do the same analysis and find the upper bound.

We apply the same strategy and compare our result for the  $Z'_{SSM}$  model with the one by the CMS collaboration [52, 62]. According to the CMS analysis, we integrate the differential

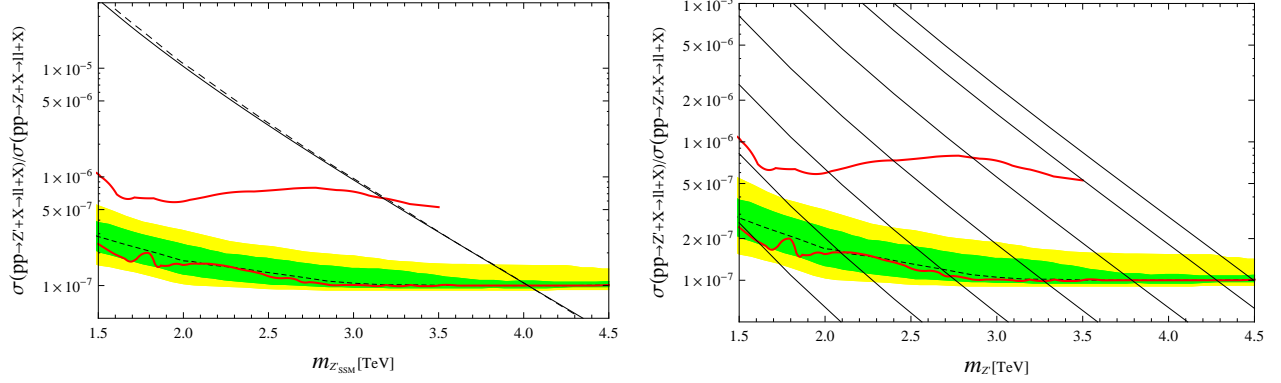


FIG. 4. Left panel: the cross section ratio as a function of the  $Z'_{SSM}$  mass (solid line) with  $k = 1.61$ , along with the CMS results in 2015 [62] and 2016 [52] from the combined di-electron and di-muon channels. Right panel: the cross section ratios calculated for various values of  $\alpha_X$  with  $k = 1.61$  for  $x_H = 0$ . The solid lines from left to right correspond to  $\alpha_X = 10^{-4.5}, 10^{-4}, 10^{-3.5}, 10^{-3}, 10^{-2.5}, 10^{-2}$ , and  $10^{-1.75}$ , respectively.

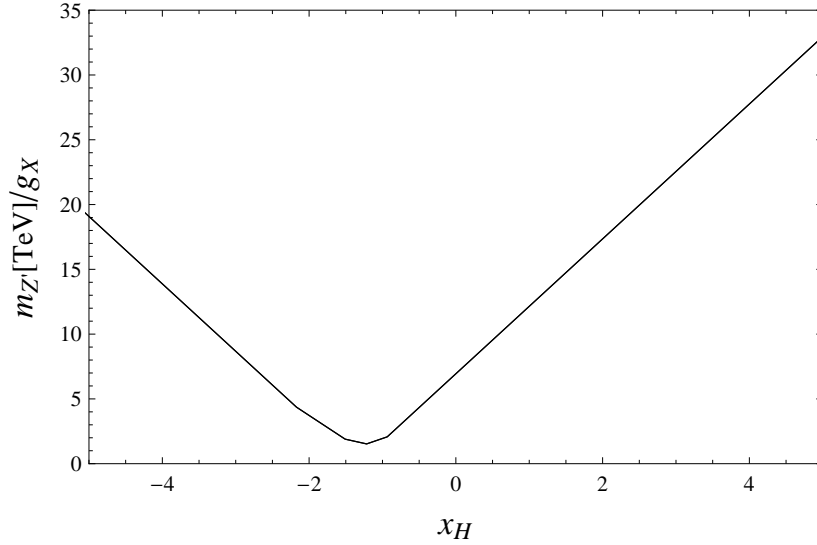


FIG. 5. The lower bound on  $m_{Z'}/g_X$  as a function of  $x_H$ . We have employed the final LEP 2 data [55] at 95% confidence level.

cross section in the range of  $0.95 \leq M_{\ell\ell}/m_{Z'_{SSM}} \leq 1.05$ . In the CMS analysis, a limit has been set on the ratio of the  $Z'_{SSM}$  boson cross section to the  $Z/\gamma^*$  cross section in a mass window of 60 to 120 GeV, which is predicted to be 1928 pb. Our result is shown as a diagonal solid line in the left panel of Fig. 4, along with the plot presented in Ref. [52]. The analysis in this CMS paper leads to the lower limit of the  $Z'_{SSM}$  boson mass as 4.0 TeV, which is read off from the intersection point of the theoretical prediction (diagonal dashed line) and the experimental

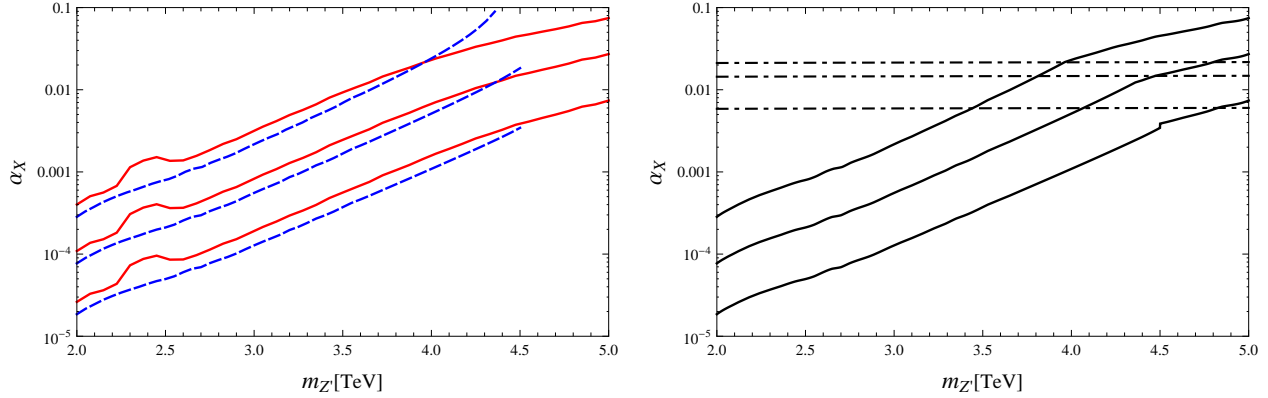


FIG. 6. Left panel: the upper bounds on  $\alpha_X$  as a function of  $m_{Z'}$  for  $x_H = -1, 0$  and  $+1$  from top to bottom for both of the solid and dashed lines, respectively. The solid lines denote the bounds from the ATLAS results [51] while the dashed lines denote the bounds from the CMS results [52]. Right panel: the upper bounds on  $\alpha_X$  after combining the ATLAS and the CMS results shown in the left panel. The solid lines correspond to the combined upper bounds for  $x_H = -1, 0$  and  $+1$  from top to bottom, respectively. The perturbativity bounds of Eq. (17) for  $x_H = -1, 0$  and  $+1$  are shown as the horizontal dashed-dotted lines from top to bottom, respectively.

cross section bound (lower horizontal solid curve (in red)). Here, we have also shown the plot presented in Ref. [62] (upper horizontal solid curve (in red)). As in the left panel of Fig. 3, we can see the dramatic improvement from the 2015 results [62] to the 2016 results [52]. In order to obtain the same lower mass limit of  $m_{Z'_{SSM}} \geq 4.0$  TeV, we have introduced a factor  $k = 1.61$ . We can see that our result (solid line) are very consistent with the theoretical cross section (dashed line) presented in Ref. [52].

With the factor of  $k = 1.61$ , we have calculated the cross section of the process  $pp \rightarrow Z' + X \rightarrow \ell^+ \ell^- + X$  for various values of  $\alpha_X$ ,  $m_{Z'}$  and  $x_H$ . For the minimal  $B-L$  model limit, we show our results in the right panel of Fig. 4, along with the plots in the CMS papers [52, 62]. The diagonal solid lines from left to right correspond to  $\alpha_X = 10^{-4.5}, 10^{-4}, 10^{-3.5}, 10^{-3}, 10^{-2.5}, 10^{-2}$ , and  $10^{-1.75}$ . From the intersections of the lower horizontal curve and the diagonal solid lines, we can read off the lower bounds on the  $Z'$  boson mass for the corresponding  $\alpha_X$  values. For example,  $m_{Z'} > 3.8$  TeV for  $\alpha_X = 10^{-2.5}$ . In this way, we have obtained the upper bound on  $\alpha_X$  as a function of the  $Z'$  boson mass. For various values of  $x_H$  we do the same analysis and find the upper bound.

The search for effective 4-Fermi interactions mediated by a  $Z'$  boson at the LEP leads to a lower bound on  $m_{Z'}/g_X$  [54, 55]. Employing the limits from the final LEP 2 data [55] at 95% confidence level, we follow Ref. [63] and derive a lower bound on  $m_{Z'}/g_X$  as a function of  $x_H$ .

Our result is shown in Fig. 5. For example, we find

$$\frac{m_{Z'}}{g_X} \geq 6.94 \text{ TeV}. \quad (16)$$

for the minimal  $B - L$  model limit, which is consistent with the result found in Ref. [64]. We find that for any values of  $x_H$ , the LEP constraints are always weaker than the LHC Run-2 constraints for  $m_{Z'} \leq 5 \text{ TeV}$ .

As a theoretical constraint, we may impose an upper bound on the  $U(1)_X$  gauge coupling to avoid the Landau pole in its renormalization group evolution  $\alpha_X(\mu)$  up to the Plank mass,  $1/\alpha_X(M_{Pl}) > 0$ , where  $M_{Pl} = 1.22 \times 10^{19} \text{ GeV}$ . Let us define the gauge coupling  $\alpha_X$  used in our analysis for the dark matter physics and LHC physics as the running gauge coupling  $\alpha_X(\mu)$  at  $\mu = m_{Z'}$ . Employing the renormalization group equation at the one-loop level with  $m_N^1 = m_N^2 = m_\Phi = m_{Z'}$ , for simplicity, we find

$$\alpha_X < \frac{2\pi}{b_X \ln \left[ \frac{M_{Pl}}{m_{Z'}} \right]}, \quad (17)$$

where  $b_X = (72 + 64x_H + 41x_H^2)/6$  is the beta function coefficient.

In Fig. 6 we show the LHC Run-2 bounds on  $\alpha_X$  as a function of  $m_{Z'}$  for  $x_H = -1, 0$  and  $+1$ . In the left panel, the solid (dashed) lines from top to bottom denote the upper bounds on  $\alpha_X$  for  $x_H = -1, 0$  and  $+1$ , respectively, obtained from the ATLAS results [51] (the CMS results [52]). For  $m_{Z'} \lesssim 4 - 4.5 \text{ TeV}$ , the CMS bounds are slightly more severe than those from the ATLAS results. Combining the ATLAS and the CMS results, we obtain the upper bound shown in the right panel. The solid lines corresponds to the combined upper bounds for  $x_H = -1, 0$  and  $+1$  from top to bottom, respectively. The perturbativity bounds of Eq. (17) for  $x_H = -1, 0$  and  $+1$  are shown as the horizontal dashed-dotted lines from top to bottom, respectively.

## V. COMPLEMENTARITY BETWEEN THE COSMOLOGICAL AND THE LHC CONSTRAINTS

Now we combine the constraints that we have obtained in the previous two sections. The RHN DM abundance has led to the lower bound on the  $U(1)_X$  gauge coupling for fixed  $m_{Z'}$  and  $x_H$ , while the upper limit on the production cross section of the  $Z'$  boson at the LHC has derived the upper bound on the gauge coupling. Therefore, the two constraints are complementary to each other and, once combined, the model parameter space is more severely constrained.

We show the results for various  $x_H$  values in Fig. 7. The top-left panel shows the results for the minimal  $B - L$  model limit ( $x_H = 0$ ). The (black) solid line shows the lower bound on  $\alpha_X$

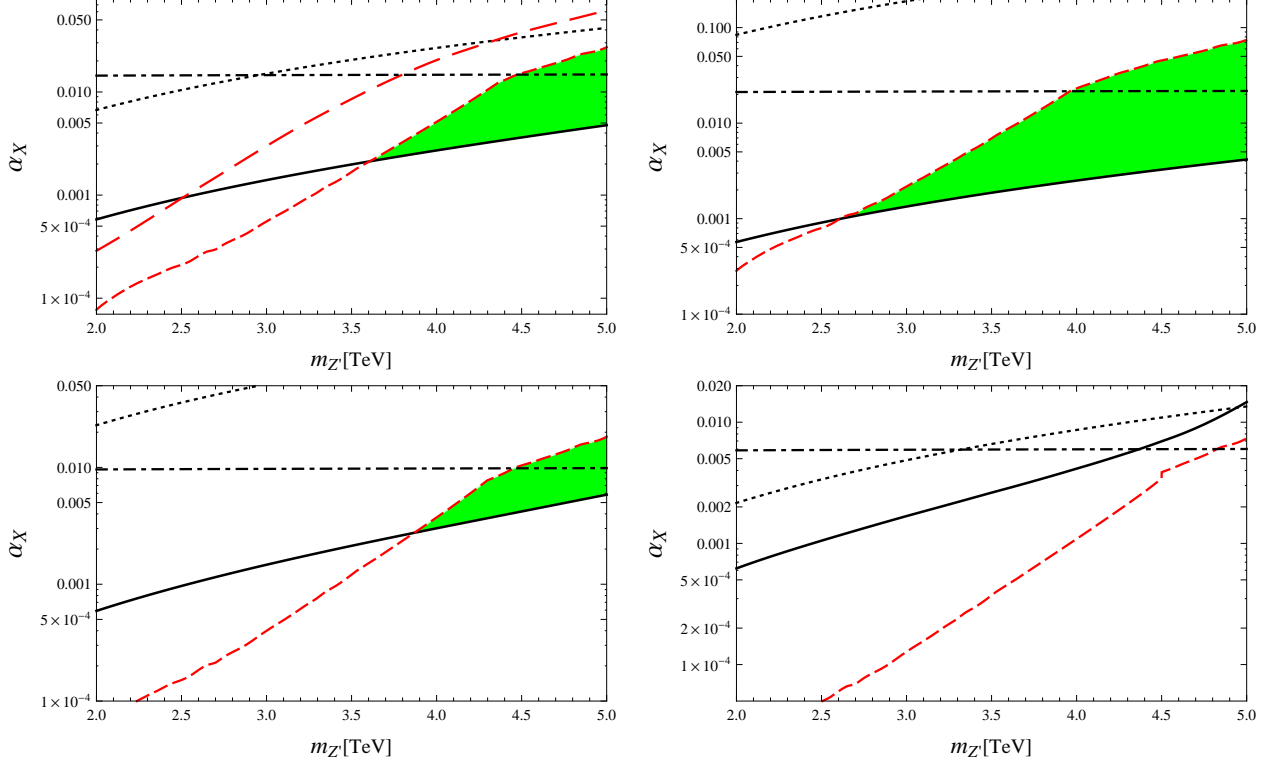


FIG. 7. Allowed parameter region for the  $Z'$ -portal RHN DM scenario. The top-left panel shows the results for the minimal  $B - L$  model limit ( $x_H = 0$ ). The (black) solid line denotes the lower bound on  $\alpha_X$  as a function of  $m_{Z'}$  to reproduce the observed DM relic abundance. The lower dashed line (in red) shows the upper bound on  $\alpha_X$  obtained from the search results for  $Z'$  boson resonance at the LHC. The shaded region is the final result after combining the cosmological and the LHC constraints, leading to the lower mass bound of  $m_{Z'} \gtrsim 3.6$  TeV. For a comparison, we have also shown the upper long-dashed line (in red) obtained in Ref. [40] by using the LHC results in 2015. The LEP upper bound in Eq. (16) is depicted as the dotted line. We also show the perturbativity bound on  $\alpha_X$  as the dashed-dotted line. The top-right, the bottom-left and the bottom-right panels are same as the top-left panel, but  $x_H = -1, -2$  and  $+1$ , respectively.

as a function of  $m_{Z'}$  to reproduce the observed DM relic abundance. The lower dashed line (in red) shows the upper bound on  $\alpha_X$  obtained from the search results for  $Z'$  boson resonance by the ATLAS [51] and the CMS [52] collaborations. Here, the ATLAS and the CMS bounds are combined as in the right panel on Fig. 6. The shaded region is the final result after combining the cosmological and the LHC constraints, leading to the lower mass bound of  $m_{Z'} \gtrsim 3.6$  TeV. For a comparison, we have also shown the upper long-dashed line (in red), which is obtained in Ref. [40] from the ATLAS [60] and the CMS [62] results with the 2015 data. We can see the dramatic improvement from the previous result of  $m_{Z'} \gtrsim 2.5$  TeV. The upper bound on  $\alpha_X$  from the LEP constraint in Eq. (16) is depicted as the dotted line, which turns out to be

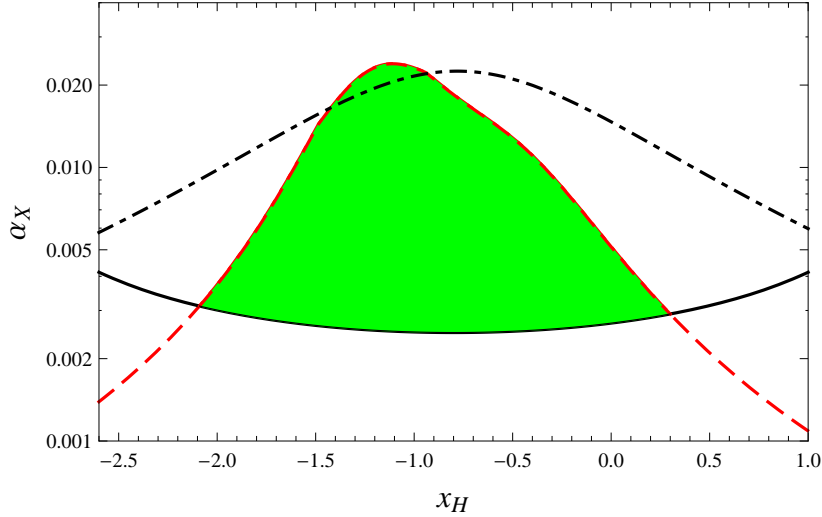


FIG. 8. Allowed parameter region for the  $Z'$ -portal RHN DM scenario for  $m_{Z'} = 4$  TeV. The (black) solid line shows the cosmological lower bound on  $\alpha_X$  as a function of  $x_H$ . The dashed line (in red) shows the upper bound on  $\alpha_X$  obtained from the combined ATLAS and CMS bounds. The shaded region is the final result for the allowed parameter space after combining the cosmological and the LHC constraints, leading to the allowed range of  $-2.1 \leq x_H \leq 0.3$ . The LEP bound appears above the plot range. The dashed-dotted line denotes the theoretical upper bound on  $\alpha_X$  in Eq. (17).

weaker than the LHC bound. We also show the theoretical upper bound on  $\alpha_X$  in Eq. (17) as the dashed-dotted line. If we impose this bound, it provides the most severe upper bound for the range of  $4.5 \text{ TeV} \lesssim m_{Z'} \lesssim 5.0 \text{ TeV}$ . In Fig. 7, the top-right, the bottom-left and the bottom-right panels are same as the top-left panel, but  $x_H = -1, -2$  and  $+1$ , respectively. We find that the largest allowed region is obtained for  $x_H \simeq -1$ , while no allowed region has been found for a  $x_H$  value outside the range of  $-2.5 \leq x_H \leq 1$ .

Finally, for a fixed  $m_{Z'} = 4$  TeV, we show the allowed parameter region in Fig. 8. The (black) solid line shows the lower bound on  $\alpha_X$  as a function of  $x_H$  to reproduce the observed DM relic abundance. As discussed in Sec. III, the minimum  $\alpha_X$  appears at  $x_H \simeq -0.8$ . The dashed line (in red) shows the upper bound on  $\alpha_X$  obtained from the combined ATLAS and CMS constraints. The shaded region is the final result for the allowed parameter space after combining the cosmological and the LHC constraints, leading to the allowed range of  $-2.1 \leq x_H \leq 0.3$ . The LEP upper bound appears above the plot range. The dashed-dotted line denotes the theoretical upper bound from the perturbativity of the running  $\alpha_X(\mu)$  up to the Planck scale.

The maximum value of  $\alpha_X$  to satisfy the LHC bound appears at  $x_H \simeq -1$ . This means that the cross section of the  $Z'$  boson production at the LHC exhibits its minimum at  $x_H \simeq -1$ .

This fact can be roughly understood by using the narrow width approximation. When the decay width of the  $Z'$  boson is very narrow, we approximate Eq. (14) as

$$\hat{\sigma}(q\bar{q} \rightarrow Z' \rightarrow \ell^+\ell^-) \simeq \frac{\pi}{1296} \alpha_X^2 M_{\ell\ell}^2 \left[ \frac{\pi}{m_{Z'} \Gamma_{Z'}} \delta(M_{\ell\ell}^2 - m_{Z'}^2) \right] F_{q\ell}(x_H) \propto \frac{F_{q\ell}(x_H)}{F(x_H)}. \quad (18)$$

Using the explicit formulas for  $F(x_H)$  and  $F_{q\ell}(x_H)$  given in Eqs. (10) and (15), we can verify that the function  $F_{q\ell}(x_H)/F(x_H)$  exhibits a minimum at  $x_H \simeq -1$ .

## VI. CONCLUSIONS

We have considered the minimal non-exotic  $U(1)_X$  extension of the SM, which is free from all the gauge and the gravitational anomalies in the presence of three right-handed neutrinos. After the breaking of the  $U(1)_X$  and the electroweak gauge symmetries, the SM neutrino masses and flavor mixings are generated through the seesaw mechanism. We have extended this model by introducing a  $Z_2$ -parity and assigned an odd-parity to one RHN while even-parities to all the other particles. Thanks to the parity, the  $Z_2$ -odd RHN is stable and hence the DM candidate. No extension of the minimal particle content is necessary to incorporate a DM candidate into the model. With the other two RHNs, the seesaw mechanism works to account for the neutrino oscillation data with one massless neutrino. In this model, the RHN DM communicates with the SM particles through the  $Z'$  boson exchange. We have investigated this  $Z'$ -portal RHN DM scenario in this paper.

Phenomenology of the scenario is controlled by only four free parameters, namely, the  $U(1)_X$  gauge coupling ( $\alpha_X$ ), the RHN DM mass ( $m_{DM}$ ), the  $Z'$  boson mass ( $m_{Z'}$ ) and the  $U(1)_X$  charge of the SM Higgs doublet field ( $x_H$ ). We have first considered the cosmological constraint of the scenario. In order to reproduce the observed DM relic density, we have found it necessary to enhance the DM annihilation cross section via  $Z'$  boson resonance. Therefore, the RHN DM mass is always set to be  $m_{DM} \simeq m_{Z'}/2$ , and the number of the free parameters is reduced to three. The three parameters are constrained by the DM relic abundance. For example, the lower bound on  $\alpha_X$  has been obtained as a function of  $m_{Z'}$  for a fixed  $x_H$ . We have next considered the LHC constraints on the  $Z'$  boson production cross section by employing the most recent results by the ATLAS and the CMS collaborations on the search for a narrow resonance with the di-lepton final state. We have derived the lower bound on  $\alpha_X$  as a function of  $m_{Z'}$  for a fixed  $x_H$ . In constraining the model parameter space, the cosmological and the LHC bounds are complementary with each other, and we have narrowed the phenomenologically viable parameter region by combining them. For example, we have found the lower limit of the  $Z'$  boson mass to be  $m_{Z'} \gtrsim 2.7$  TeV. In our analysis, we have also taken into account other

phenomenological constraints such as the LEP bound on the  $U(1)_X$  symmetry breaking scale and the perturbativity bound on the running  $U(1)_X$  gauge coupling below the Planck scale.

## ACKNOWLEDGMENTS

We would like to thank Ryusuke Endo for valuable discussions and comments. We also wish to thank Digesh Raut for reading the manuscript and his useful comments. S.O. is very grateful to Andy Okada for his encouragements. She would also like to thank the Department of Physics and Astronomy at the University of Alabama for hospitality during her visit for the completion of this work. The work of N.O. is supported in part by the United States Department of Energy (Award No. de-sc0013680).

- 
- [1] R. N. Mohapatra and R. E. Marshak, “Local B-L Symmetry of Electroweak Interactions, Majorana Neutrinos and Neutron Oscillations,” *Phys. Rev. Lett.* **44** (1980) 1316–1319. [Erratum: *Phys. Rev. Lett.* 44,1643(1980)].
  - [2] R. E. Marshak and R. N. Mohapatra, “Quark - Lepton Symmetry and B-L as the  $U(1)$  Generator of the Electroweak Symmetry Group,” *Phys. Lett.* **B91** (1980) 222–224.
  - [3] C. Wetterich, “Neutrino Masses and the Scale of B-L Violation,” *Nucl. Phys.* **B187** (1981) 343–375.
  - [4] A. Masiero, J. F. Nieves, and T. Yanagida, “B-L Violating Proton Decay and Late Cosmological Baryon Production,” *Phys. Lett.* **B116** (1982) 11–15.
  - [5] R. N. Mohapatra and G. Senjanovic, “Spontaneous Breaking of Global B-L Symmetry and Matter-Antimatter Oscillations in Grand Unified Theories,” *Phys. Rev.* **D27** (1983) 254.
  - [6] W. Buchmuller, C. Greub, and P. Minkowski, “Neutrino masses, neutral vector bosons and the scale of B-L breaking,” *Phys. Lett.* **B267** (1991) 395–399.
  - [7] P. Minkowski, “ $\mu \rightarrow e\gamma$  at a Rate of One Out of  $10^9$  Muon Decays?,” *Phys. Lett.* **B67** (1977) 421–428.
  - [8] T. Yanagida, “HORIZONTAL SYMMETRY AND MASSES OF NEUTRINOS,” *Conf. Proc.* **C7902131** (1979) 95–99.
  - [9] M. Gell-Mann, P. Ramond, and R. Slansky, “Complex Spinors and Unified Theories,” *Conf. Proc.* **C790927** (1979) 315–321, [arXiv:1306.4669 \[hep-th\]](#).
  - [10] S. L. Glashow, “The Future of Elementary Particle Physics,” *NATO Sci. Ser.* **B61** (1980) 687.
  - [11] R. N. Mohapatra and G. Senjanovic, “Neutrino Mass and Spontaneous Parity Violation,” *Phys. Rev. Lett.* **44** (1980) 912.
  - [12] N. Okada and O. Seto, “Higgs portal dark matter in the minimal gauged  $U(1)_{B-L}$  model,” *Phys. Rev.* **D82** (2010) 023507, [arXiv:1002.2525 \[hep-ph\]](#).
  - [13] A. Anisimov and P. Di Bari, “Cold Dark Matter from heavy Right-Handed neutrino mixing,” *Phys. Rev.* **D80** (2009) 073017, [arXiv:0812.5085 \[hep-ph\]](#).
  - [14] S. F. King, “Large mixing angle MSW and atmospheric neutrinos from single right-handed neutrino dominance and  $U(1)$  family symmetry,” *Nucl. Phys.* **B576** (2000) 85–105,

- arXiv:hep-ph/9912492 [hep-ph].
- [15] P. H. Frampton, S. L. Glashow, and T. Yanagida, “Cosmological sign of neutrino CP violation,” *Phys. Lett.* **B548** (2002) 119–121, arXiv:hep-ph/0208157 [hep-ph].
  - [16] M. Fukugita and T. Yanagida, “Baryogenesis Without Grand Unification,” *Phys. Lett.* **B174** (1986) 45–47.
  - [17] N. Okada and Y. Orikasa, “Dark matter in the classically conformal B-L model,” *Phys. Rev.* **D85** (2012) 115006, arXiv:1202.1405 [hep-ph].
  - [18] T. Basak and T. Mondal, “Constraining Minimal  $U(1)_{B-L}$  model from Dark Matter Observations,” *Phys. Rev.* **D89** (2014) 063527, arXiv:1308.0023 [hep-ph].
  - [19] H. An, X. Ji, and L.-T. Wang, “Light Dark Matter and  $Z'$  Dark Force at Colliders,” *JHEP* **07** (2012) 182, arXiv:1202.2894 [hep-ph].
  - [20] H. An, R. Huo, and L.-T. Wang, “Searching for Low Mass Dark Portal at the LHC,” *Phys. Dark Univ.* **2** (2013) 50–57, arXiv:1212.2221 [hep-ph].
  - [21] D. E. Soper, M. Spannowsky, C. J. Wallace, and T. M. P. Tait, “Scattering of Dark Particles with Light Mediators,” *Phys. Rev.* **D90** (2014) no. 11, 115005, arXiv:1407.2623 [hep-ph].
  - [22] D. Aristizabal Sierra, F. Staub, and A. Vicente, “Shedding light on the  $b \rightarrow s$  anomalies with a dark sector,” *Phys. Rev.* **D92** (2015) no. 1, 015001, arXiv:1503.06077 [hep-ph].
  - [23] Z. M. Burell and N. Okada, “Supersymmetric minimal B-L model at the TeV scale with right-handed Majorana neutrino dark matter,” *Phys. Rev.* **D85** (2012) 055011, arXiv:1111.1789 [hep-ph].
  - [24] L. Basso, O. Fischer, and J. J. van der Bij, “Natural Z model with an inverse seesaw mechanism and leptonic dark matter,” *Phys. Rev.* **D87** (2013) no. 3, 035015, arXiv:1207.3250 [hep-ph].
  - [25] M. Das and S. Mohanty, “Leptophilic dark matter in gauged  $L_\mu - L_\tau$  extension of MSSM,” *Phys. Rev.* **D89** (2014) no. 2, 025004, arXiv:1306.4505 [hep-ph].
  - [26] X. Chu, Y. Mambrini, J. Quevillon, and B. Zaldivar, “Thermal and non-thermal production of dark matter via  $Z'$ -portal(s),” *JCAP* **1401** (2014) 034, arXiv:1306.4677 [hep-ph].
  - [27] E. Dudas, L. Heurtier, Y. Mambrini, and B. Zaldivar, “Extra  $U(1)$ , effective operators, anomalies and dark matter,” *JHEP* **11** (2013) 083, arXiv:1307.0005 [hep-ph].
  - [28] M. Lindner, D. Schmidt, and A. Watanabe, “Dark matter and  $U(1)$ ’ symmetry for the right-handed neutrinos,” *Phys. Rev.* **D89** (2014) no. 1, 013007, arXiv:1310.6582 [hep-ph].
  - [29] A. Alves, S. Profumo, and F. S. Queiroz, “The dark  $Z'$  portal: direct, indirect and collider searches,” *JHEP* **04** (2014) 063, arXiv:1312.5281 [hep-ph].
  - [30] J. Kopp, L. Michaels, and J. Smirnov, “Loopy Constraints on Leptophilic Dark Matter and Internal Bremsstrahlung,” *JCAP* **1404** (2014) 022, arXiv:1401.6457 [hep-ph].
  - [31] P. Agrawal, Z. Chacko, and C. B. Verhaaren, “Leptophilic Dark Matter and the Anomalous Magnetic Moment of the Muon,” *JHEP* **08** (2014) 147, arXiv:1402.7369 [hep-ph].
  - [32] D. Hooper, “ $Z'$  mediated dark matter models for the Galactic Center gamma-ray excess,” *Phys. Rev.* **D91** (2015) 035025, arXiv:1411.4079 [hep-ph].
  - [33] E. Ma and R. Srivastava, “Dirac or inverse seesaw neutrino masses with B-L gauge symmetry and  $S_3$  flavor symmetry,” *Phys. Lett.* **B741** (2015) 217–222, arXiv:1411.5042 [hep-ph].
  - [34] A. Alves, A. Berlin, S. Profumo, and F. S. Queiroz, “Dark Matter Complementarity and the  $Z'$  Portal,” *Phys. Rev.* **D92** (2015) no. 8, 083004, arXiv:1501.03490 [hep-ph].
  - [35] K. Ghorbani and H. Ghorbani, “Two-portal Dark Matter,” *Phys. Rev.* **D91** (2015) no. 12, 123541, arXiv:1504.03610 [hep-ph].

- [36] B. L. Sanchez-Vega and E. R. Schmitz, “Fermionic dark matter and neutrino masses in a B-L model,” *Phys. Rev.* **D92** (2015) 053007, [arXiv:1505.03595 \[hep-ph\]](#).
- [37] M. Duerr, P. Fileviez Perez, and J. Smirnov, “Simplified Dirac Dark Matter Models and Gamma-Ray Lines,” *Phys. Rev.* **D92** (2015) no. 8, 083521, [arXiv:1506.05107 \[hep-ph\]](#).
- [38] A. Alves, A. Berlin, S. Profumo, and F. S. Queiroz, “Dirac-fermionic dark matter in  $U(1)_X$  models,” *JHEP* **10** (2015) 076, [arXiv:1506.06767 \[hep-ph\]](#).
- [39] E. Ma, N. Pollard, R. Srivastava, and M. Zakeri, “Gauge B-L Model with Residual  $Z_3$  Symmetry,” *Phys. Lett.* **B750** (2015) 135–138, [arXiv:1507.03943 \[hep-ph\]](#).
- [40] N. Okada and S. Okada, “ $Z'_{BL}$  portal dark matter and LHC Run-2 results,” *Phys. Rev.* **D93** (2016) no. 7, 075003, [arXiv:1601.07526 \[hep-ph\]](#).
- [41] N. Okada and N. Papapietro, “R-parity Conserving Minimal SUSY B-L Model,” [arXiv:1603.01769 \[hep-ph\]](#).
- [42] W. Chao, H.-k. Guo, and Y. Zhang, “Majorana Dark matter with B+L gauge symmetry,” [arXiv:1604.01771 \[hep-ph\]](#).
- [43] A. Biswas, S. Choubey, and S. Khan, “Galactic gamma ray excess and dark matter phenomenology in a  $U(1)_{B-L}$  model,” *JHEP* **08** (2016) 114, [arXiv:1604.06566 \[hep-ph\]](#).
- [44] E. Accomando, C. Coriano, L. Delle Rose, J. Fiaschi, C. Marzo, and S. Moretti, “ $Z'$ , Higgses and heavy neutrinos in  $U(1)'$  models: from the LHC to the GUT scale,” *JHEP* **07** (2016) 086, [arXiv:1605.02910 \[hep-ph\]](#).
- [45] M. Fairbairn, J. Heal, F. Kahlhoefer, and P. Tunney, “Constraints on Z models from LHC dijet searches and implications for dark matter,” *JHEP* **09** (2016) 018, [arXiv:1605.07940 \[hep-ph\]](#).
- [46] K. Kaneta, Z. Kang, and H.-S. Lee, “Right-handed neutrino dark matter under the B-L gauge interaction,” [arXiv:1606.09317 \[hep-ph\]](#).
- [47] M. Klasen, F. Lyonnet, and F. S. Queiroz, “NLO+NLL Collider Bounds, Dirac Fermion and Scalar Dark Matter in the B-L Model,” [arXiv:1607.06468 \[hep-ph\]](#).
- [48] P. S. B. Dev, R. N. Mohapatra, and Y. Zhang, “Naturally Stable Right-Handed Neutrino Dark Matter,” [arXiv:1608.06266 \[hep-ph\]](#).
- [49] W. Altmannshofer, S. Gori, S. Profumo, and F. S. Queiroz, “Explaining Dark Matter and  $B$  Decay Anomalies with an  $L_\mu - L_\tau$  Model,” [arXiv:1609.04026 \[hep-ph\]](#).
- [50] T. Appelquist, B. A. Dobrescu, and A. R. Hopper, “Nonexotic neutral gauge bosons,” *Phys. Rev.* **D68** (2003) 035012, [arXiv:hep-ph/0212073 \[hep-ph\]](#).
- [51] **ATLAS** Collaboration, “Search for new high-mass resonances in the dilepton final state using proton-proton collisions at  $\sqrt{s} = 13$  TeV with the ATLAS detector,” ATLAS-CONF-2016-045 .
- [52] **CMS** Collaboration, “Search for a high-mass resonance decaying into a dilepton final state in  $13 \text{ fb}^{-1}$  of pp collisions at  $\sqrt{s} = 13$  TeV,” CMS-PAS-EXO-16-031 .
- [53] S. Iso, N. Okada, and Y. Orikasa, “Resonant Leptogenesis in the Minimal B-L Extended Standard Model at TeV,” *Phys. Rev.* **D83** (2011) 093011, [arXiv:1011.4769 \[hep-ph\]](#).
- [54] **SLD Electroweak Group, SLD Heavy Flavor Group, DELPHI, LEP, ALEPH, OPAL, LEP Electroweak Working Group, L3** Collaboration, “A Combination of preliminary electroweak measurements and constraints on the standard model,” [arXiv:hep-ex/0312023 \[hep-ex\]](#).
- [55] **DELPHI, OPAL, LEP Electroweak, ALEPH, L3** Collaboration, S. Schael *et al.*, “Electroweak Measurements in Electron-Positron Collisions at W-Boson-Pair Energies at LEP,”

- Phys. Rept. **532** (2013) 119–244, [arXiv:1302.3415 \[hep-ex\]](#).
- [56] **Planck** Collaboration, N. Aghanim *et al.*, “Planck 2015 results. XI. CMB power spectra, likelihoods, and robustness of parameters,” *Astron. Astrophys.* **594** (2016) A11, [arXiv:1507.02704 \[astro-ph.CO\]](#).
- [57] **ATLAS** Collaboration, G. Aad *et al.*, “Search for high-mass dilepton resonances in pp collisions at  $\sqrt{s} = 8$  TeV with the ATLAS detector,” *Phys. Rev.* **D90** (2014) no. 5, 052005, [arXiv:1405.4123 \[hep-ex\]](#).
- [58] **CMS** Collaboration, “Search for Resonances in the Dilepton Mass Distribution in pp Collisions at  $\sqrt{s} = 8$  TeV,” CMS-PAS-EXO-12-061 (2013) .
- [59] J. Pumplin, D. R. Stump, J. Huston, H. L. Lai, P. M. Nadolsky, and W. K. Tung, “New generation of parton distributions with uncertainties from global QCD analysis,” *JHEP* **07** (2002) 012, [arXiv:hep-ph/0201195 \[hep-ph\]](#).
- [60] **ATLAS** Collaboration, “Search for new phenomena in the dilepton final state using proton-proton collisions at  $\sqrt{s} = 13$  TeV with the ATLAS detector,” ATLAS-CONF-2015-070 .
- [61] V. D. Barger, W.-Y. Keung, and E. Ma, “Doubling of Weak Gauge Bosons in an Extension of the Standard Model,” *Phys. Rev. Lett.* **44** (1980) 1169.
- [62] **CMS** Collaboration, “Search for a Narrow Resonance Produced in 13 TeV pp Collisions Decaying to Electron Pair or Muon Pair Final States,” CMS-PAS-EXO-15-005 .
- [63] M. Carena, A. Daleo, B. A. Dobrescu, and T. M. P. Tait, “ $Z'$  gauge bosons at the Tevatron,” *Phys. Rev.* **D70** (2004) 093009, [arXiv:hep-ph/0408098 \[hep-ph\]](#).
- [64] J. Heck, “Unbroken B-L symmetry,” *Phys. Lett.* **B739** (2014) 256–262, [arXiv:1408.6845 \[hep-ph\]](#).